

The DTT device: Poloidal field coil assessment for alternative plasma configurations



R. Ambrosino^{a,*}, R. Albanese^b, G. Calabrò^c, A. Castaldo^b, F. Crisanti^c, V.P. Loschiavo^b, M. de Magistris^b, S. Minucci^b, G. Ramogida^c

^a Consorzio CREATE and Dip. di Ingegneria, Università degli Studi di Napoli Parthenope, Centro Direzionale di Napoli, Isola C4, 80143 Napoli, Italy

^b Consorzio CREATE and DIETI, Università degli Studi di Napoli Federico II, Via Claudio 21, I-80125 Napoli, Italy

^c ENEA Unità Tecnica Fusione, C.R. Frascati, Via E. Fermi 45, I-00044 Frascati, Roma, Italy

ARTICLE INFO

Article history:

Received 21 July 2016

Received in revised form

29 December 2016

Accepted 29 January 2017

Available online 24 February 2017

Keywords:

Tokamak

Plasma magnetic configurations

Alternative divertor concepts

ABSTRACT

This paper firstly illustrates the objectives, the figure of merits and the specifications considered in the design of the equilibrium configurations in the Divertor Tokamak Test (DTT) facility. The reference single null scenario is detailed. The range of alternative plasma shapes and current capabilities are then discussed. A number of in-vessel coils can be used to locally modify the magnetic configuration in the divertor region. Finally, a comparison of costs and benefits of the various configurations is given, with particular reference to the power exhaust issues.

© 2017 EURATOM. Published by Elsevier B.V. All rights reserved.

1. Introduction

The main objective of the Divertor Tokamak Test (DTT) facility is to host experiments addressed to the solution of the power exhaust issues in view of DEMO [1]. This derives from the need to develop integrated and controllable exhaust solutions including plasma, PFCs, control diagnostics and actuators, using experiments, theory and modelling, so as to mitigate the risk that conventional divertor might not be suitable for DEMO [1].

The requirements are detailed in [2] and include:

- specifications on a number of normalized plasma parameters relevant for DEMO.
- ratio between power crossing the separatrix P_{sep} and the major radius R relevant for DEMO ($P_{\text{sep}}/R \geq 15 \text{ MW/m}$).
- flexibility in the divertor region so as to possibly test different divertors.
- possibility to test alternative magnetic configurations.
- possibility to test liquid metals.
- integrated scenarios (solutions to be compatible with plasma performance and technological constraints of DEMO).
- budget constraint (500 M€).

* Corresponding author.

E-mail address: roberto.ambrosino@uniparthenope.it (R. Ambrosino).

These requirements led to the selection of the following parameters: a major radius of 2.15 m, an aspect ratio of about 3, an elongation of about 1.7, a toroidal field of 6 T, a plasma current of 6 MA, and a flat top of about 100 s [3].

Promising experimental results on alternative configurations have been obtained in DIII-D [4], EAST [5], MAST [6], NSTX [7] and TCX [8–10]. The DTT device addresses the challenge of investigate alternative magnetic configurations including snowflake, quasi-snowflake, double null, and negative triangularity equilibria with plasma conditions similar to DEMO. The behavior of such alternative configurations will be compared with the reference single null.

The Super-X divertor concept seeks to maximize the major radius of the divertor targets, R_t [11]. However, the maximum value is limited by the toroidal field coils. A Super-X configuration with a major radius of 2.15 m would have been incompatible with the budget constraint. However, long-leg configurations at low plasma current might also be considered in the future.

The paper is structured as follows. Section 2 illustrates the objectives, the figure of merits and the specifications considered in the design of the equilibrium configurations. Section 3 reports the reference single null scenario. Section 4 describes the alternative configurations that can be achieved in DTT. Section 5 show how the in-vessel coils can be used to locally modify the magnetic configuration in the divertor region. Section 6 compares the costs

and benefits of the various configurations and illustrates the main conclusions of the paper.

2. Objectives, figures of merit and specifications

The main specifications considered for the design of the plasma scenario are hereafter summarized. They include constraints on the plasma, on the poloidal field (PF) coils, on the central solenoid (CS).

2.1. PF/CS coil currents

The PF coil system considered for the plasma scenarios is reported in Table 1. The minor differences with respect to [3] are mainly related to the fact that the current is considered as uniformly distributed over the cross section including strands, void and jackets. The PF/CS coil positions and cross sections have been designed with an iterative procedure taking into account the above specifications as well as the geometrical constraints related to the locations of ports and TF coils. Table 2 reports voltage and current limits for these coils [3].

Table 1
PF Coil System Used for MHD Calculations.

Name	R (m)	Z (m)	ΔR (m)	ΔZ (m)	Turns
CS3U	0.6685	2.2615	0.343	0.635	270
CS2U	0.6685	1.458	0.343	0.972	420
CS1U	0.6685	0.486	0.343	0.972	420
CS1L	0.6685	-0.486	0.343	0.972	420
CS2L	0.6685	-1.458	0.343	0.972	420
CS3L	0.6685	-2.2615	0.343	0.635	270
PF1	1.34	2.23	0.377	0.32	130
PF2	3.49	1.931	0.468	0.174	108
PF3	4.28	0.745	0.192	0.49	112
PF4	4.15	-1.049	0.245	0.469	140
PF5	3.25	-2.45	0.494	0.228	152
PF6	1.541	-2.76	0.754	0.32	260
C1	1.44	-1.481	0.07	0.07	1
C2	1.74	-1.823	0.07	0.07	1
C3	2	-1.925	0.07	0.07	1
C4	2.18	-1.668	0.07	0.07	1
C5	3.1	-0.83	0.14	0.14	4
C6	3.285	0.51	0.14	0.14	4
C7	2.988	-1.15	0.07	0.07	1
C8	2.915	1.25	0.07	0.07	1

Table 2
Voltage and Current Limits (four quadrants).

Name	I_{sat} (kA)	V_{sat} (V)	Turns
CS3U	23	800	270
CS2U	23	800	420
CS1U	23	800	420
CS1L	23	800	420
CS2L	23	800	420
CS3L	23	800	270
PF1	25.2	800	130
PF2	22.6	800	108
PF3	21.2	1000	112
PF4	24.7	1000	140
PF5	23	800	152
PF6	23.3	800	260
C1	60	50	1
C2	60	50	1
C3	60	50	1
C4	60	50	1
C5	25	200	4
C6	25	200	4
C7	60	50	1
C8	60	50	1

*These limits are for the currents in the scenario: the plasma shape control system can use additional 2.0 kA in PF2-PF3-PF4-PF5 and additional 1.0 kA in PF1 and PF6.

2.2. Magnetic field

The maximum magnetic field at the location of the CS coils shall not exceed 12.5 T. The constraint related to the magnetic field is not stringent for the PF coils. A posteriori, it was verified that its maximum value is about 4.0 T in PF6.

2.3. Vertical forces on the PF/CS coils

The force limits on the PF coils are scaled from DEMO constraints [12]. We assume the force scaling with the square of RB_{tor} . In DEMO the toroidal field B_{tor} is 7 T and the major radius R is 9 m [13], therefore we assume a reduction of a factor of 24 with respect to DEMO. Thus, the maximum vertical force on the central solenoid stack in DTT should not exceed 12.5 MN, the maximum separation force in the central solenoid stack should not exceed 14.5 MN and the maximum vertical force on a single PF coil should be 19 MN.

The forces on the in-vessel coils are scaled from ITER [15], where the maximum force is 744 kN/m and the maximum current is 240 kA (up to 320 kA in short transients). Since in DTT we assume 60 kA, the maximum force should be reduced to 186 kN/m. Therefore, the limits of ± 4 MN for the vertical force are taken for the coils connected to other structures (vacuum vessel or divertor) via rails or other means.

2.4. Plasma

The maximum plasma current is 6 MA, whereas the plasma shape parameters should be similar to the present EU design of DEMO, with an aspect ratio $R/a \approx 3.1$, an elongation $k \approx 1.76$, and an average triangularity $\langle \delta \rangle \approx 0.35$ [12]. The maximum values assumed in the nominal scenarios at full current for poloidal beta β_p and internal inductance l_i are 0.5 and 1.0, respectively. The minimum plasma-wall distance shall be 40 mm, taking into account that the power decay length at 6 MA is about 2 mm at the outboard midplane. The minimum grazing angle of the magnetic field at the strike points shall be 1.5° . The pulse length should be at least 100 s, so as to overcome all thermal transients; this is guaranteed by a total available poloidal flux of about 45 Vs (CS swing of about 35 Vs and a PF contribution of about 10 Vs), not to mention the possible current drive contributions of the ECRH and the NBI system to be implemented at a later stage.

2.5. Figures of merit

The various configurations will be compared in terms of costs on the PF coil system and benefits related to the power exhaust. Due to the constraints on the maximum PF currents and vertical forces of the PF coils system, the scenarios of the alternative configurations have been designed at a different flat top plasma current with a pulse length of 100s. The power exhaust properties of the configurations are quantified in terms of poloidal flux expansion and connection length at a distance of 20 cm from the active null point, on a virtual target designed to be perpendicular to the separatrix baffles. The Scrape-Off Layer (SOL) is considered to be enclosed by a magnetic surface passing through a point placed 2 mm (i.e., the power decay length) outside the plasma at the outboard midplane.

3. Reference single null scenario

Table 3 shows the time evolution of the PF coil currents, along with the plasma geometrical and physical parameters guaranteeing the sequence of plasma shapes during a pulse. It defines the DTT reference Single Null (SN) scenario, obtained by using the CREATE-NL code [16] in combination with FIXFREE code [17].

Table 3
Reference Single Null (SN) Scenario.

Time [s]	0.000	0.020	15.000	22.000	27.000	32.000	42.000	100.000
I_p [MA]	0.000	0.000	3.000	4.300	6.000	6.000	6.000	6.000
β_p	0.000	0.000	0.098	0.100	0.100	0.100	0.430	0.430
l_i	0.000	0.000	0.984	0.876	0.876	0.876	0.895	0.895
Ψ_b [Vs]	17.810	17.440	8.936	5.762	4.522	3.693	2.838	-5.588
Configuration	–	–	Limiter	X-point	X-point	X-point	X-point	X-point
ICS3U [MAturns]	6.220	6.061	0.720	0.560	0.280	0.160	0.190	-0.760
ICS2U [MAturns]	9.670	9.423	2.660	1.840	0.210	-0.330	-0.950	-9.180
ICS1U [MAturns]	9.670	9.423	2.000	-1.600	-4.160	-4.530	-4.710	-9.180
ICS1L [MAturns]	9.670	9.423	2.510	-3.670	-7.040	-7.460	-7.150	-9.180
ICS2L [MAturns]	9.670	9.423	2.190	3.420	2.440	1.980	1.030	-9.180
ICS3L [MAturns]	6.220	6.061	0.440	1.580	1.770	1.590	1.590	1.310
IPF1 [MAturns]	1.680	1.637	0.640	0.490	0.310	0.210	0.310	0.270
IPF2 [MAturns]	0.710	0.692	-0.040	-0.180	-0.400	-0.440	-0.410	-0.710
IPF3 [MAturns]	0.000	0.000	-0.930	-1.130	-1.580	-1.580	-1.940	-2.050
IPF4 [MAturns]	0.000	0.000	-0.790	-1.990	-2.740	-2.740	-2.830	-2.370
IPF5 [MAturns]	0.740	0.721	0.190	-0.150	-0.310	-0.310	-0.350	-1.510
IPF6 [MAturns]	2.350	2.290	0.900	3.480	4.130	3.950	3.920	3.990
IC5 [kA]	0.00	9.97	0.00	0.00	0.00	0.00	0.00	0.00
IC6 [kA]	0.00	15.15	0.00	0.00	0.00	0.00	0.00	0.00
growth rate ^a (s ⁻¹)	–	–	–	39	39	37	42	34
stability margin ^a	–	–	–	0.52	0.52	0.53	0.47	0.55

^a Calculated with axisymmetric models ignoring the effects of first wall and ports.

As shown in Fig. 1, a good field null during the plasma breakdown (i.e., a large central hexapolar region even at low field) is guaranteed. The toroidal electric field for breakdown has been imposed to be 1.5 V/m for a duration of at least 20 ms.

The scenario has been designed so as to provide the necessary flux (~ 35 Vs stored) and to build-up the X-point configuration for the 6MA H-mode reference scenario. For this case, the discharge lasts around 100 s from the breakdown to the end of flat top with the X-point configuration sustained (at low and/or high beta) for ~ 75 s (much longer than the plasma resistive time). The central solenoid (CS) column is split in six different coils to allow the largest plasma shaping flexibility.

After the breakdown, the plasma current I_p rises up to 3.0 MA in $\Delta t = 15$ s; during this phase, the plasma evolves with a circular to elliptical shape, leaning on the inboard side of the first wall, where the tungsten thickness is planned to be increased by a factor of two. Between $t = 15$ s and $t = 22$ s the plasma current ramps up to 4.3 MA achieving the X-point configuration. In this scenario the plasma remains limited for about 15 s. This is not at all a machine constraint. The coils and power supply flexibility will allow experiments (at full performance) where the limited phase can be reduced to a few seconds.

Between $t = 22$ s and $t = 27$ s, the plasma current achieves its target value of 6 MA, while β_p remains very low. At $t = 32$ s, full additional heating is assumed, causing an increase of the internal kinetic energy on a time scale longer than the plasma energy confinement time. After $t = 42$ s, all plasma physical parameters are assumed to remain nearly constant up to the end of the current plateau at $t = 100$ s. During the flat top with a plasma current of 6 MA and a toroidal field of 6 T, the plasma volume is 33 m³, whereas the safety factor is $q_{axis} = 1.0$ at the magnetic axis, and $q_{95} = 2.8$ at 95% of the magnetic poloidal flux. The maximum heating power in all cases (SN or advanced divertor configurations) is assumed to be the 45 MW, provided by a mix of three different systems the ICRH, the ECRH and NNBI, described in [18]. This reference scenario makes reference to a 40 MW additional heating power.

At the end of flat top, the plasma is no longer heated and a controlled ramp-down phase similar to the JET tokamak follows, in which the plasma current decreases at the rate of 100 kA/s (up to 500 kA/s if needed in emergency cases) while keeping a single null configuration at low beta, low elongation, and controlled density (no more than 50% of Greenwald limit) till about 200 kA; then the

plasma configuration becomes limited, leaning on the inboard wall, where the plasma current decreases to zero.

The scenario is compatible with a duty cycle considering 30–60 min between two pulses. The configurations satisfy the PF system limits reported in Section 2 and keep a minimum distance of 40 mm between the plasma last closed surface and the first wall in the diverted phase, in order to minimize the interaction between the plasma and the main chamber.

The boundary flux Ψ_{SOF} at start of flat top ($t = 27$ s) is calculated assuming an Ejima coefficient $C_{EJIMA} = 0.4$ and a breakdown flux $\Psi_{BD} = 18$ Vs [19]:

$$\Psi_{SOF} = \Psi_{BD} - (0.5 \mu_0 R l_i I_p + C_{EJIMA} \mu_0 R l_i I_p) = 4.5 \text{ Vs} \quad (1)$$

Enough space has been allocated in the divertor region, not only to substantially vary the plasma divertor magnetic topology, but also to allow strike point sweeping and to have an efficient pumping capability. In addition, the full divertor can be removed by remote handling to allow tests based on different divertor geometries and/or liquid metals. The foreseen large input power, together with the estimated short energy e-folding length, required to carefully evaluate the divertor heat loads expected in DTT. To comply with this request, numerical self-consistent simulations have been made for the H-mode by using the 2D multi-fluid code COREDIV [20]. The impact of unmitigated giant (around 1.2 MJ) type I Edge Localized Modes (ELMs) on DTT divertor targets was also analysed.

It should be noted that for optimizing the local divertor magnetic configuration, DTT will be equipped with a set of internal coils, capable to adjust a second null generated by the PF external coils and obtain X-Divertor (where the flaring can be largely varied) and Snow Flake configurations (with a wide region where B_p and its gradient are very low), as discussed in Section 5.

Finally, the feedback control system should be capable to:

- stabilize the vertical position
- keep the shape at steady state within ~ 2 cm from its reference in case of current density profile changes (within $\Delta\beta \sim \pm 0.2$ and $\Delta l_i \sim \pm 0.1$)
- for diverted configuration keep the plasma-wall clearance at least ~ 4 cm at steady state and ~ 1 cm during transients of about ~ 1 s.

Two internal coils (C5–C6) are foreseen for vertical and horizontal fast feed-back control. Detailed analyses have been performed to

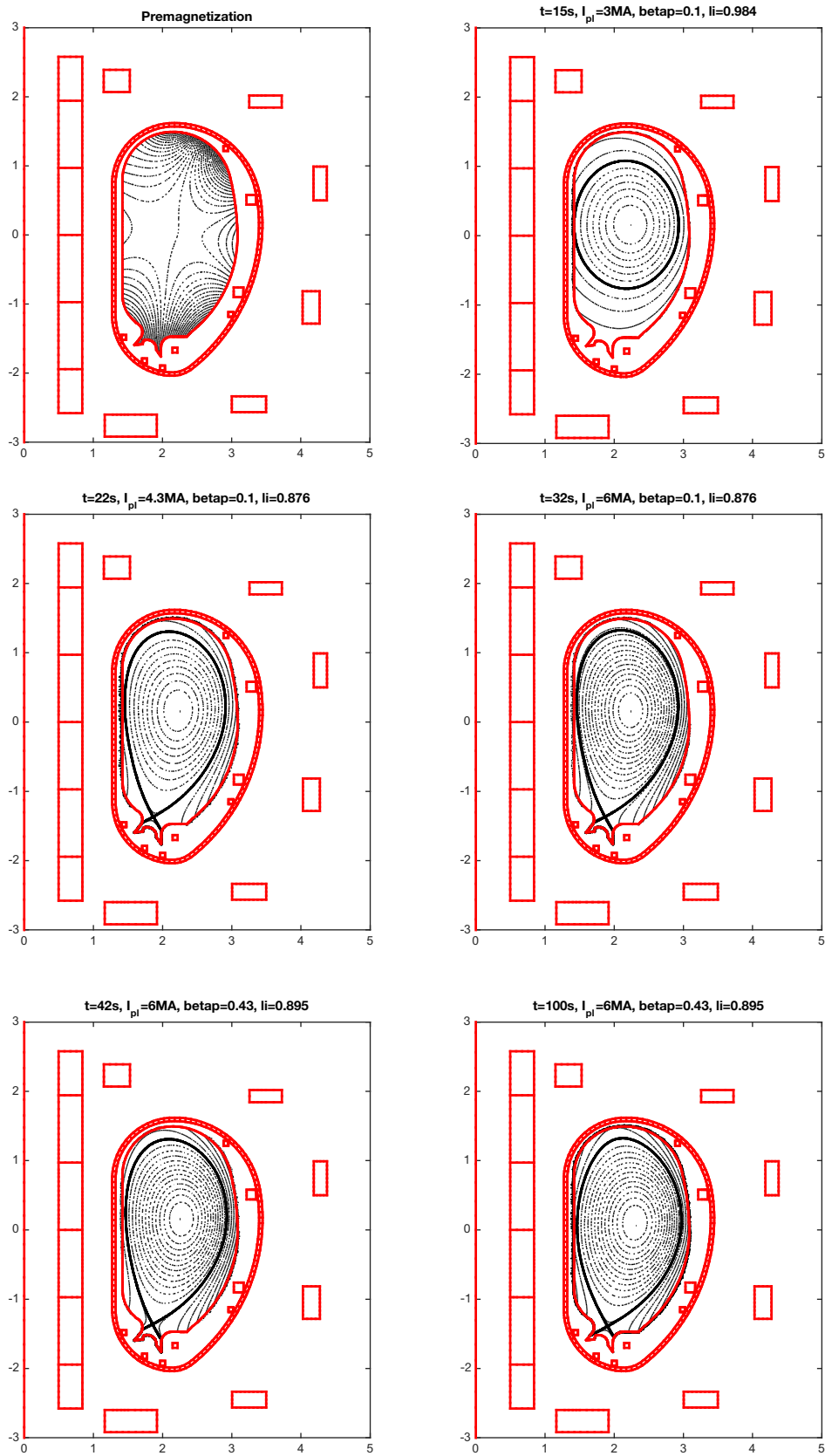


Fig. 1. DTT H-mode reference scenario: at $t=22s$ X-point formation with $I_p = 4.3MA$, at $t=27s$ with $I_p = 6MA$ at low β_p and finally at $t=32s$ with $I_p = 6MA$ at high β_p .

Table 4
Alternative configurations at flat top.

Configuration Phase	SF		SF ⁺		DN		RT	
	SOF	EOF	SOF	EOF	SOF	EOF	SOF	EOF
I _p [MA]	4	4	5	5	5	5	5	5
β _p	0.430	0.430	0.430	0.430	0.430	0.430	0.430	0.430
Li	0.895	0.895	0.895	0.895	0.895	0.895	0.895	0.895
Ψ _b [Vs]	7.606	-3.920	3.07	-4.38	2.681	-5.168	2.623	-5.121
ICS3U [MAtorns]	0.372	-5.691	5.86	4.46	5.900	2.484	0.206	-1.016
ICS2U [MAtorns]	3.739	3.538	1.17	-1.94	-0.103	-5.950	0.345	-2.626
ICS1U [MAtorns]	0.429	-8.742	-4.09	-9.18	-5.506	-9.177	-2.647	-9.177
ICS1L [MAtorns]	-4.400	-9.177	-6.55	-9.18	-6.304	-9.177	-8.352	-9.177
ICS2L [MAtorns]	7.728	0.037	2.51	-3.21	-2.350	-9.177	-0.631	-9.177
ICS3L [MAtorns]	4.968	0.980	5.90	3.91	2.795	0.868	2.863	1.044
IPF1 [MAtorns]	0.123	-3.042	-1.65	-2.80	2.992	2.809	0.142	-1.125
IPF2 [MAtorns]	0.473	0.857	0.14	-0.55	-2.003	-2.615	-0.265	-0.591
IPF3 [MAtorns]	-1.594	-2.266	-2.06	-1.37	-1.220	-0.968	-2.027	-1.895
IPF4 [MAtorns]	-3.034	-2.782	-2.95	-3.45	-1.151	-1.136	-2.685	-2.856
IPF5 [MAtorns]	2.839	2.383	1.87	1.75	-2.779	-3.165	2.320	1.969
IPF6 [MAtorns]	-0.901	-2.322	-0.65	-1.62	5.616	4.893	-0.185	-0.275
IC5 [kA]	-	-	-	-	-	-	-	-
IC6 [kA]	-	-	-	-	-	-	-	-
Plasma volume (m ³)	36	36	39	39	36	37	41	41
growth rate ^a (s ⁻¹)	123	233	86	59	124	60	70	64
stability margin ^a	0.18	0.10	0.25	0.36	0.18	0.34	0.30	0.32

^a Calculated with axisymmetric models ignoring the effects of first wall and ports.

study the control of the plasma current, shape and position during the flat-top of the reference H-mode plasma scenario [26].

4. Alternative configurations for DTT

DTT capabilities include various alternative configurations (ACs), including ideal snowflake (SF), quasi snowflake (SF⁺ and SF⁻), X-divertor (XD), double null (DN), and negative triangularity (NT) plasmas (Fig. 2 and Table 4). The divertor structure in Figs. 1–2 refers to the reference single null configuration; the design of a divertor structure compatible with the alternative configurations is under analysis [21].

The snowflake divertor concept seeks to decrease the poloidal field in the vicinity of the null point by introducing a second order null point [22]. This splits the separatrix around the null into six legs with two enclosing the confined plasma and four divertor legs. Since the exact SFD is only a point in the operational plane any real configuration is characterized by two nearby X-points [23]. The resulting configuration may have different topologies referred to snowflake plus (SFD⁺) and snowflake minus (SFD⁻) depending on whether the second x-point is located in the private or common flux region of the primary, active x-point, respectively. A potentially undesirable consequence is an increase of the poloidal flux compression towards the target (in contrast to the XD). The lower poloidal field in the null point region leads to a longer connection length and divertor volume and is expected to generate large volumetric losses.

The DN plasmas decrease the inner wall heat load and split the average load between the upper and lower outboard targets with suitable plasma wobbling. However, the share is not guaranteed in the transient phases and therefore the outboard targets have to be designed taking into account the peak loads. The PF coil system of DTT is capable to sustain a high current (5 MA) double null configuration for a long flat top (more than 40 s). The double null configuration can be tested in the first phase of the scientific programme at low current and/or in L-mode. In a second phase it can be tested for short periods also in H-mode with suitable precaution so as to prevent damages to the upper part of the first wall (e.g., short duration, wobbling, sweeping, or suitable reinforcement plates). However, a significant double null experiment should be carried out not only with a symmetric magnetic configuration (which is feasi-

ble) but also with an up-down symmetric structure of the divertor and pumping system. For this reason, particular care will be taken in the design of a modular first wall, so as to allow removing it and mounting another divertor in the upper part of the machine (whenever required by the future scientific programme).

The PF coil system of DTT is also capable to sustain a significant plasma current with a reverse triangularity in the divertor region for a sufficiently long flat top. This configuration, which slightly improves the magnetic flux expansion of the inner leg, can be tested in the first phase of the scientific programme at low current and/or in L-mode. In a second phase it can be tested for short periods also in H-mode with an alternative divertor or, with suitable precautions, with the nominal divertor, which is not optimized for this case.

Any configuration can be obtained via specific scenarios, or alternatively, during the flat top of a reference scenario (at full or reduced current) by means of a transition for SN to AC and vice versa. These configurations verify current, field, vertical force and plasma-wall distance constraints. Moreover, relaxing the vertical force constraints up to 30 MN, it is also possible to define a SF scenario with a flat top plasma current of I_{p1} = 5.5 MA (instead of 4 MA), as illustrated in Fig. 3. A Super-X configuration with a major radius of 2.15 m would have been incompatible with the budget constraint, however, long-leg configurations at low plasma current might also be considered in the future. Finally, possible optimization of SF, SF⁺ and XD configurations can be obtained using the internal coils C1–C8, as illustrated in Section 5.

5. Use of in-vessel coils

The study of the divertor physics and technology is one of the main target of the DTT. Indeed, for optimizing the local magnetic configuration and consequently controlling various parameters related to the power exhaust (flux expansion, connection length, distance between null points, etc.), DTT will be equipped with a set of internal coils capable to locally modify the magnetic field in the vicinity of the divertor target. Using these in-vessel coils, it will be possible to adjust a second null region in Snowflake-like configurations, obtaining a large area where B_p and its gradient are close to zero or defining XD-like configuration where the flux flaring at target can be largely varied. As example of the flexibility of a such system, the SF⁺ equilibrium at SOF (Table 4), shown in (Fig. 4a), has

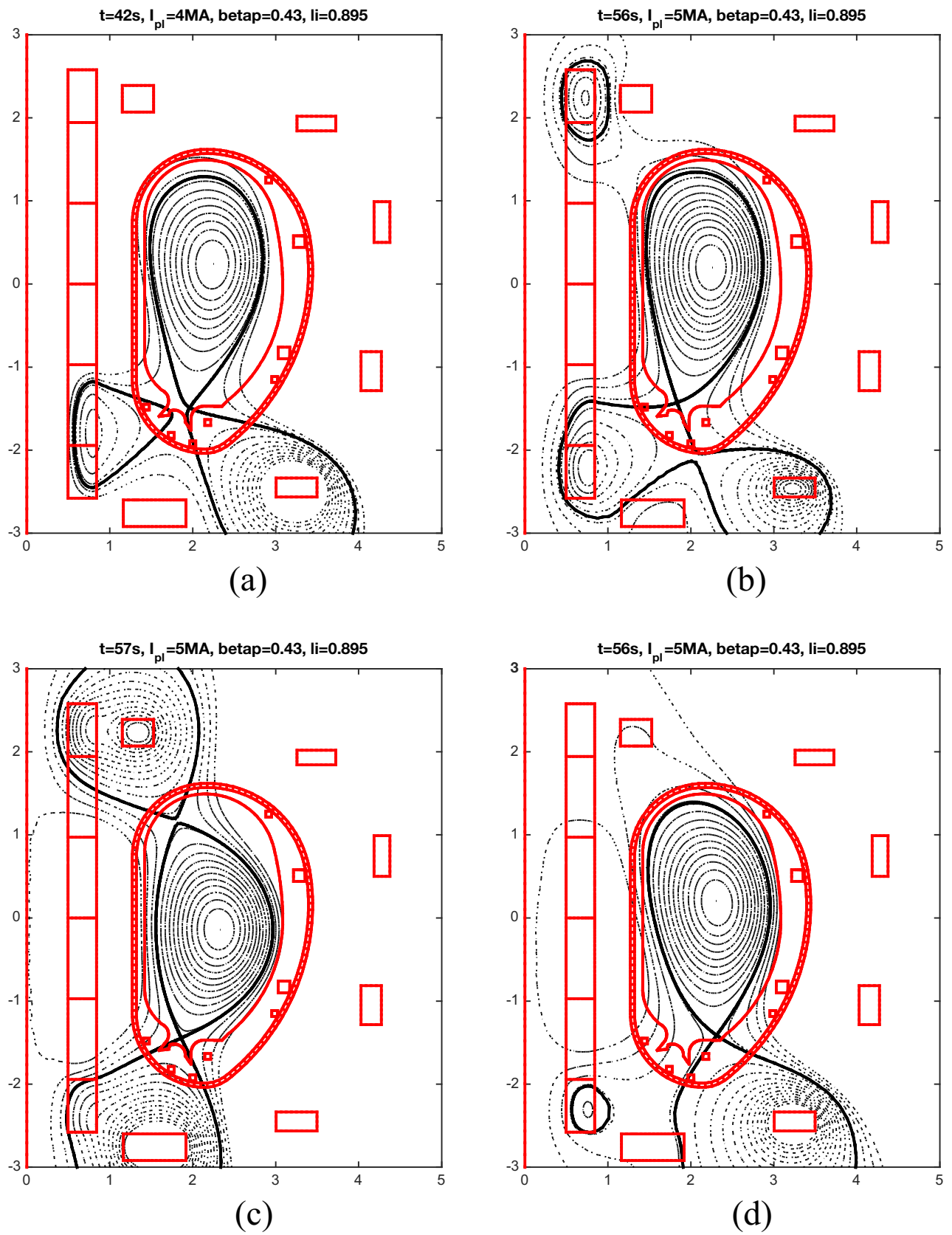


Fig. 2. Alternative configurations at SOF: a) SF; b) SF+; c) DN; d) RT.

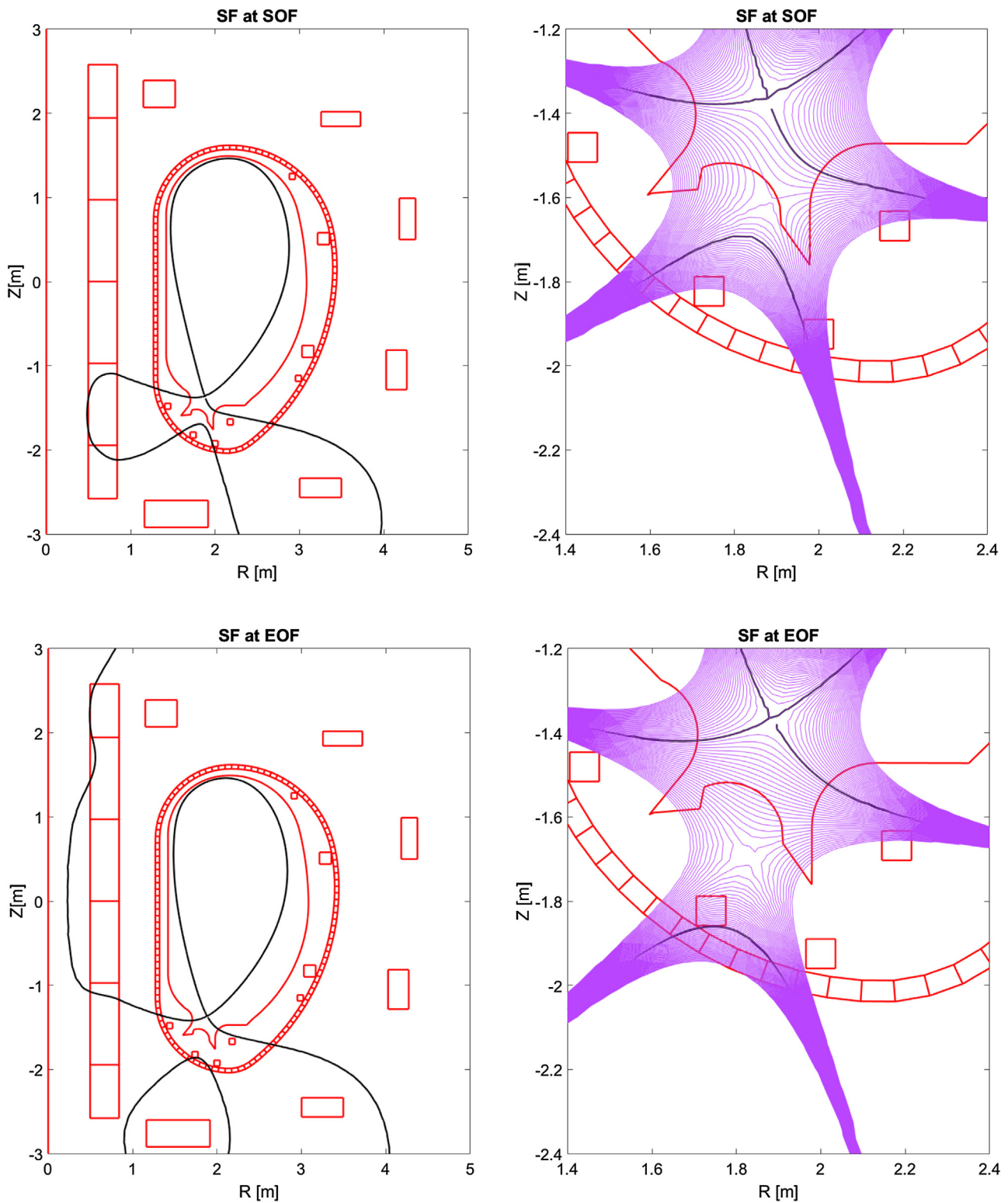


Fig. 3. SF configuration at SOF (top) and EOF (bottom) with a flat top plasma current of 5.5 MA, a flat top swing of 6.5 Vs and a maximum vertical force on the PF coils ≤ 30 MN.

been considered as starting point in our analysis with no current flowing in the internal coils C1–C4. An advanced SF⁻ configuration can be obtained by using the in-vessel coils, as shown in (Fig. 4b), modifying the distance and the poloidal flux difference between the two nulls from SF⁺ (Fig. 4c) to SF⁻ (Fig. 4d) and consequently modifying the flux flaring around the main null, characterized by the magnetic field gradient. Indeed, the dependence of ∇B_p (the

gradient of the poloidal magnetic field B_p) in the primary x-point on the distance between nulls is described in [24] as criterion of interdependence between them. A self-explanatory way to show the aforementioned dependence is to plot the iso-contours of B_p around the nulls, as discussed in [24,5], for the SF configurations with and without in-vessel coils (Fig. 4c–d). A direct manifestation of the interdependence between the nulls is that the flux flaring

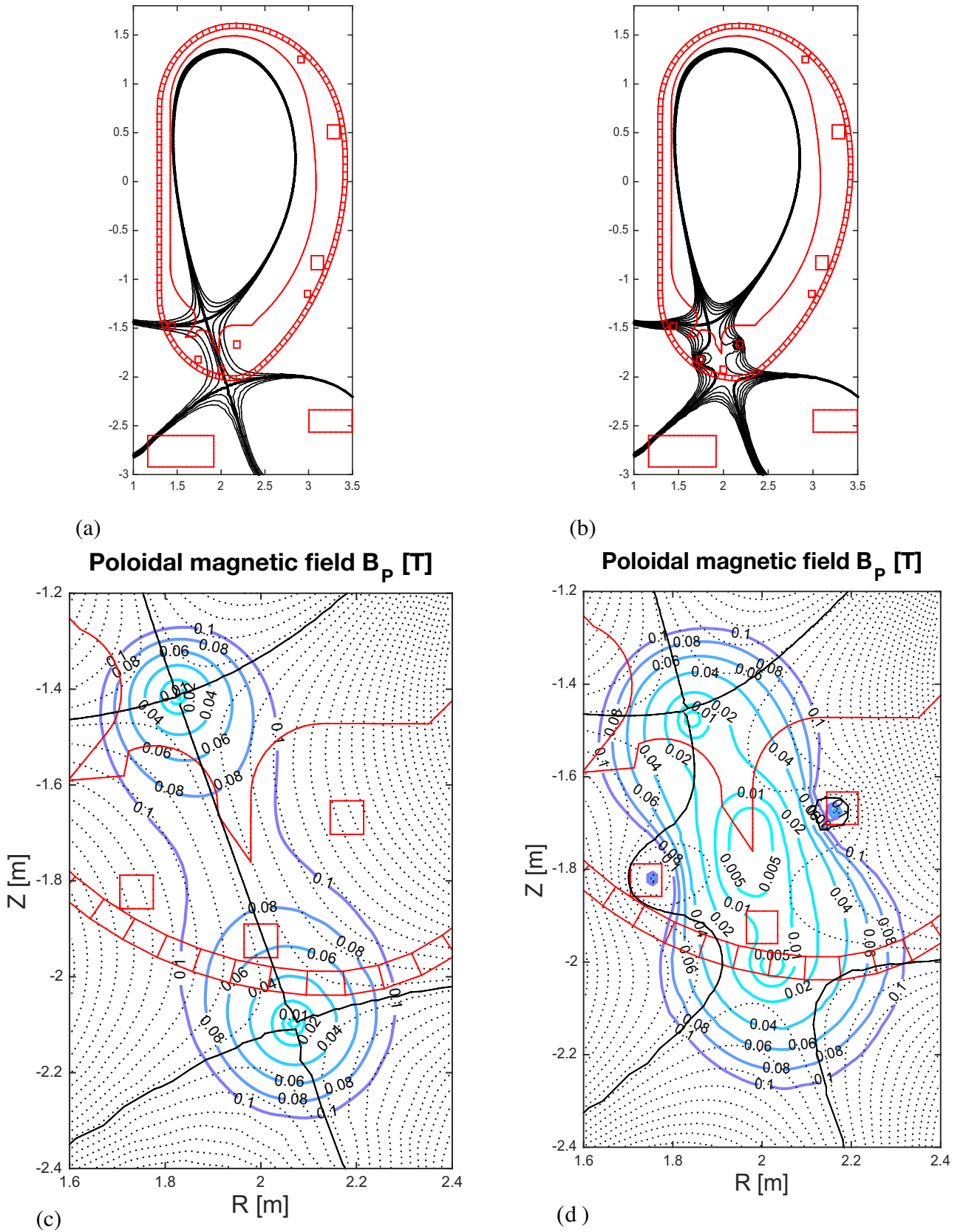


Fig. 4. Use of internal coils C1–C4 for the modification of the SF+ configuration into a SF- configuration. a) SF+ equilibrium at SOF in Table 4 b) SF- equilibrium generated from the reference SF+ with the use of the internal coils; C1 = 28.7 kA, C2 = -60 kA, C3 = 0.5 kA, C4 = 50.7 kA c) poloidal magnetic field of the SF+ configuration in the divertor region; d) poloidal magnetic field of the SF- configuration in the divertor region.

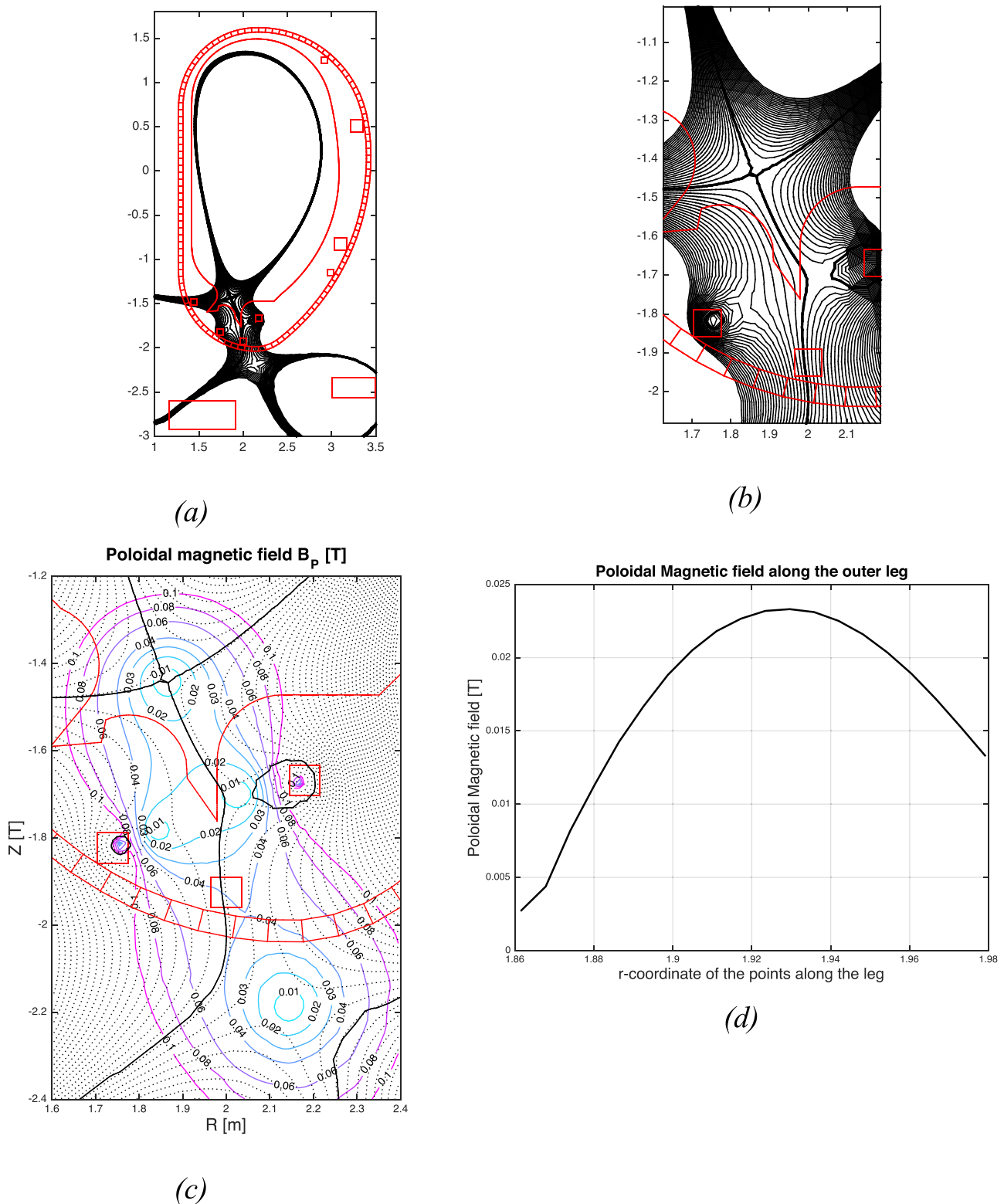


Fig. 5. Use of internal coils C1–C4 for the modification of the SF+ configuration into a XD configuration. a) XD equilibrium generated from the reference SF+ with the use of the internal coils C1 = –2.6 kA, C2 = –43.0 kA, C3 = –0.5 kA, C4 = 57.3 kA and assuming a plasma current of 4 MA b) XD equilibrium in the divertor region c) poloidal magnetic field of the XD configuration in the divertor region; d) Poloidal magnetic field along the outer leg as a function of the r-coordinate of the leg points from the X-point to the target.

(characterized by the poloidal field gradient) in the main null is affected by the presence of the second null. As shown in Fig. 4, ∇B_p depends on the distance between the nulls. This flaring is then directly translated to an increase of the main magnetic divertor

geometry parameters (poloidal flux expansion, connection length, etc.), as reported in Table 6, and consequently, to an increased wetted surface area and reduced heat flux [24].

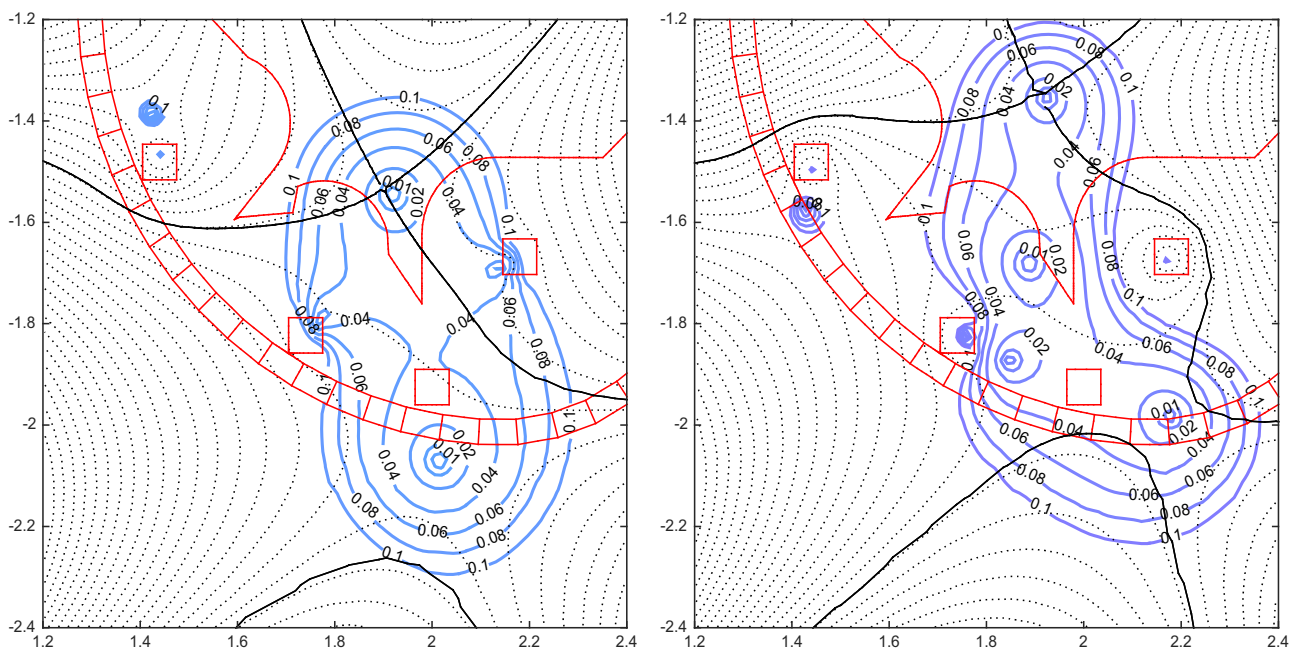


Fig. 6. DTT attractive configurations obtained by means of in-vessel coils. Poloidal magnetic field B_p [T] of the configurations.

An advanced XD configuration can be also obtained by using the lower in-vessel coils C1–C4, as shown in Fig. 5, adding a secondary X-point in the vicinity of the outer divertor plate and flaring the flux surfaces of the plate. Other attractive configurations could be further studied by means of in-vessel coils, as discussed in [25] and shown in Fig. 6, focusing on the possibility to enlarge the “flatness” B_p region around the two nulls by acting on C1–C4 currents. The current saturation at 60 kA might limit the performance of the in-vessel coil system. However, there is the possibility of doubling the cross section of each internal turn, which is feasible according to the thermal analysis reported in [11], or reducing the reference plasma current of the configuration.

In-vessel coils C5–C6 can effectively be used for plasma radial control and vertical stabilization [25]. They are also used in the breakdown phase to produce a 6 mT vertical field.

In-vessel coils C1–C4 as well as C7–C8 can be used for plasma wobbling or strike point sweeping (in any case no more than 4 internal coils will be fed in addition to C5–C6 during a pulse). The calculations show that 120 kA in C1 and C3 connected in antiseries would yield 64 mm sweeping on the outer strike point and 42 mm on the inner one. However, there are some side effects outside the vacuum vessel (e.g., 25 kA turns induced in PF6). Optimization of frequency and currents for strike point sweeping is planned in the future.

6. Cost and benefits of the configurations and final conclusions

The feasibility of SN and ACs in DTT depends on whether there are engineering solutions to achieve such configurations and how much it would cost. This section, therefore, distinguishes between *constraints* that must be met and *costs* of the configurations that are compared to the costs of the reference SN solution. The constraints of the configurations are mainly related to the maximum vertical forces of the PF/CS coils. The costs of the configurations are quantified in terms of total current request on the PF and CS coil system, related to the costs of the PF coil system, and the plasma current, the plasma volume and the flat top flux swing of the configurations, related to the expected fusion power output.

Table 5
Comparison of cost and benefits of the various configurations at flat top.

Configuration	SN	SF	SF+	DN	RT
I_p [MA]	6	4	5	5	5
Flux swing at flat top	10.11	11.53	7.45	7.85	7.74
$\Sigma I_{PF/CS} _{max}$ [MATurns] ^a	49.7	41.8	43.4	52.4	40.9
Max. force on single coil $F_{z,PF}$ (MN)	10.5	21.5	18.4	13.2	19.7
Max. vertical force on CS $F_{z,PF(total)}$ (MN)	7.6	3.4	5.3	5.7	2.1
Max. CS separation force $F_{z,PF(sep)}$ (MN)	18.7	15.9	14.9	13.4	9.0
Plasma volume (m ³)	39	36	39	36	40
Poloidal flux expansion inboard ^b	11.8	56.8	20.3	7.0	13.9
Poloidal flux expansion outboard ^b	10.9	28.9	28.7	6.3	9.9
Connection length inboard ^b	42.6	96.7	57.5	25.1	57.5
Connection length outboard ^b	23.6	45.6	40.6	21.8	25.4
growth rate $[\text{s}^{-1}]$	42	123	86	124	70
stability margin ^a	0.47	0.18	0.25	0.18	0.30

^a Calculated at SOF with axisymmetric models ignoring the effects of first wall and ports.

^b Calculated at SOF at a distance of 20 cm from the active null point with $B_T = 6T$ at $R = 2.15$ m.

The potential benefits of the configurations arise from the modified magnetic geometry. Most ACs seek to increase the connection length, the flux expansion and the SOL volume too. In this preliminary stage where the divertor design is still ongoing, the connection length and the flux expansion are evaluated at a fixed distance of 20 cm from the active null point. The connection length is evaluated assuming a SOL width on the outer equatorial plane of 2 mm (Fig. 7). Among the benefits of the configurations, the effects of the modified magnetic geometry on the vertical instability growth rate and stability margin is also considered. The evaluation of these parameters has been performed assuming axisymmetric toroidally continuous vacuum vessel neglecting the effects of the ports and of a conductive first wall.

The comparison among the various configurations in terms of constraints, costs and benefits is reported in Table 5 assuming zero current on the internal coils. Table 6 shows the effect of internal coils currents on the figures of merit of the SF+ configuration assuming fixed PF–CS coil currents. These results show that all alternative configurations are more demanding on the PF/CS coils system in terms of currents and vertical forces. Indeed, a reduced value of

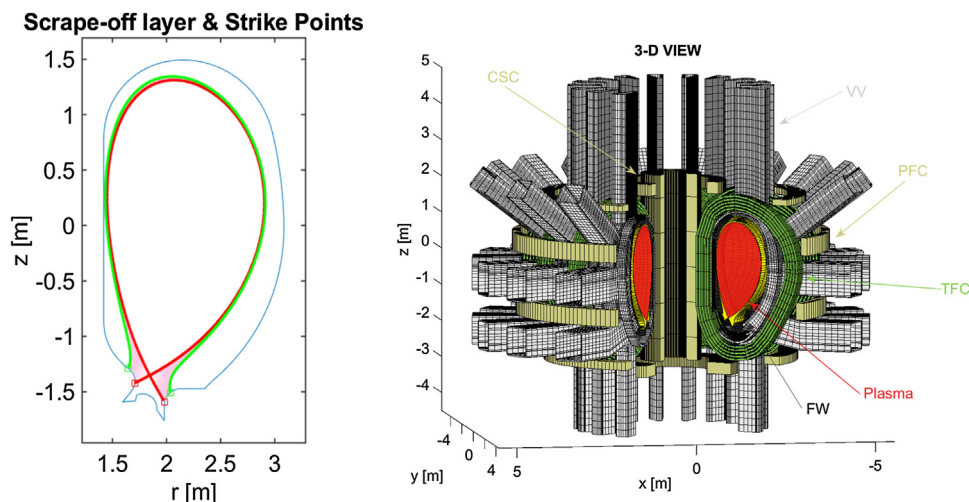


Fig. 7. 2D and 3D views of the scrape off layer for the SN configuration.

Table 6

Comparison of flux expansion and connection length of the SF plus and minus configurations with and without internal coils.

	Flux expansion IN	Flux expansion OUT	Connection Length IN	Connection Length OUT
SF+, no in-vessel coils: C1-C4=0kA	20.3	28.7	57.5	40.6
SF-, in-vessel coils: C1 = 28.7kA, C2 = -60kA, C3 = 0.5kA, C4 = 50.7kA	22.7	75.7	58.4	67.8

the plasma current has to be considered to satisfy the constraints. On the other hand, both the SF and the SF⁺ configurations yield a considerable increment of connection length and poloidal flux expansion at a fixed distance of 20 cm from the active null point. A detailed controllability analysis of the alternative configurations hasn't been performed for DTT at the present phase. However, low gradient flux surfaces in the divertor region can make some alternative configurations (SF, SF⁺ and SF⁻) more sensitive to plasma current parameters variations. These data will be useful for a proper definition of revised divertor structures optimized for the various specific configurations.

Acknowledgements

The authors gratefully thank Riccardo Lombroni for his useful contribution in the design of alternative plasma configurations.

This work has been carried out within the framework of the EUROfusion Consortium and has received funding from the Euratom research and training programme 2014–2018 under grant agreement No. 633053. The views and opinions expressed herein do not necessarily reflect those of the European Commission. Roberto Ambrosino's research was funded by the University Parthenope of Naples by means of the "Bando di sostegno alla ricerca individuale 2015–2017".

References

- [1] Fusion Electricity—A roadmap to the realisation of fusion energy, November 2012 (http://users.euro-fusion.org/iterphysics/wiki/images/9/9b/EFDA-Fusion_Roadmap_2M8JBG_v1.0.pdf).
- [2] R. Albanese, H. Reimerdes, "The DTT Device: role and objectives". Submitted to Special Issue of Fusion Engineering and Design entitled DTT: Divertor Tokamak Test facility to be published in early 2017.
- [3] F. Crisanti et al. The DTT device: choice of parameters, submitted to Special Issue of Fusion Engineering and Design entitled DTT: Divertor Tokamak Test facility to be published in early 2017.
- [4] S.L. Allen, et al., *Fusion Energy Conf., San Diego, US, 2012*.
- [5] G. Calabrò, et al., EAST alternative magnetic configurations: modelling and first experiments, *Nucl. Fusion* 55 (2015) 083005.
- [6] A.W. Morris, *IEEE Trans. Plasma Sci.* 40 (2012) 6148288.
- [7] V.A. Soukhanovskii, et al., *Phys. Plasmas* 19 (2012) 082504.
- [8] F. Piras, et al., *Plasma Phys. Control Fusion* 51 (2009) 055009.
- [9] F. Piras, et al., *Plasma Phys. Control Fusion* 52 (2010) 124010.
- [10] R. Ambrosino, et al., *Nucl. Fusion* 54 (2014) 123008.
- [11] A. Di Zenobio et al. The DTT Device: Conceptual design of the superconducting magnet system, submitted to Special Issue of Fusion Engineering and Design entitled DTT: Divertor Tokamak Test facility to be published in early 2017.
- [12] P.M. Valanju, et al., Super-X divertors and high power density fusion devices, *Phys. Plasmas* 16 (2009) 056110.
- [13] M. Mattei et al. Report on EFDA Task WP13-SYS-02: DEMO Single Null Equilibria and Vertical Stability Assessment, EFDA.D.2LM3VX, (2013).
- [15] X. Wang, F. Xie, H. Jin, Electromagnetic analysis of the ITER upper VS coil, *J. Supercond. Novel Magn.* 27 (4) (2014) 1015–1019.
- [16] R. Albanese, R. Ambrosino, M. Mattei, CREATE-NL+: a robust control-oriented free boundary dynamic plasma equilibrium solver, *Fusion Eng. Des.* 96–97 (2015) 664–667.
- [17] F. Alladio, F. Crisanti, Analysis of MHD equilibria by toroidal multipolar expansions, *Nucl. Fusion* 26 (1986) 1143.
- [18] G. Granucci et al. The DTT device: systems for heating, submitted to Special Issue of Fusion Engineering and Design entitled DTT: Divertor Tokamak Test facility to be published in early 2017.
- [19] S. Ejima, et al., Volt second analysis of D-III discharges, *Nucl. Fusion* 22 (10) (1982) 1313.
- [20] R. Zagórski et al. The DTT device: power and particle exhaust, submitted to Special Issue of Fusion Engineering and Design entitled DTT: Divertor Tokamak Test facility to be published in early 2017.
- [21] G. Maddaluno et al. The DTT device: divertor solutions for alternative configurations and liquid metals, submitted to Special Issue of Fusion Engineering and Design entitled DTT: Divertor Tokamak Test facility to be published in early 2017.
- [22] D.D. Ryutov, Geometrical properties of a snowflake divertor, *Phys. Plasmas* 14 (2007) 064502.
- [23] G. Calabrò et al. Divertor configuration with two nearby poloidal field nulls: modelling and experiments for EAST and JET tokamaks presented at 22nd International Conference on Plasma Surface Interactions in Controlled Fusion Devices, Rome, Italy 30–June 03.
- [24] D.D. Ryutov, V.A. Soukhanovskii, The snowflake divertor, *Phys. Plasmas* 22 (2015) 110901.
- [25] R. Albanese et al. DTT Facility design in view of DEMO, to be presented at IAEA DEMO Programme Workshop, 15–18 November 2016, Karlsruhe, Germany.
- [26] M. Valisa et al., The DTT device: data acquisition, diagnostics and control, submitted to Special Issue of Fusion Engineering and Design entitled DTT: Divertor Tokamak Test facility to be published in early 2017.